AGU PUBLICATIONS

Journal of Advances in Modeling Earth Systems

RESEARCH ARTICLE

10.1002/2014MS000338

Remote effect of the model cold bias in the tropical North Atlantic on the warm bias in the tropical southeastern Pacific

Liping Zhang[1,2], Chunzai Wang[3], Zhenya Song[4], and Sang-Ki Lee[3,5]

[1]Program in Atmospheric and Oceanic Sciences, Princeton University, Princeton, New Jersey, USA, [2]NOAA/Geophysical Fluid Dynamics Laboratory, Princeton, New Jersey, USA, [3]NOAA Atlantic Oceanographic and Meteorological Laboratory, Miami, Florida, USA, [4]The First Institute of Oceanography, State Oceanic Administration, Qingdao, China, [5]Cooperative Institute for Marine and Atmospheric Studies, University of Miami, Miami, Florida, USA

Key Points:
- A close link between tropical North Atlantic and southeastern Pacific SST bias
- The TNA cold bias does contribute partly to the warm SST bias in the SEP
- This link is due to the TNA-SEP Hadley cell change

Correspondence to:
L. Zhang,
ocean.climate.ping@gmail.com

Citation:
Zhang, L., C. Wang, Z. Song, and S.-K. Lee (2014), Remote effect of the model cold bias in the tropical North Atlantic on the warm bias in the tropical southeastern Pacific, *J. Adv. Model. Earth Syst.*, *6*, 1016–1026, doi:10.1002/2014MS000338.

Received 20 APR 2014
Accepted 2 OCT 2014
Accepted article online 8 OCT 2014
Published online 7 NOV 2014

Abstract Most state-of-the-art climate models show significant systematic biases in the tropical southeastern Pacific (SEP) and tropical North Atlantic (TNA). These biases manifest themselves as the sea surface temperature (SST) in the SEP being too warm and the SST in the TNA being too cold. That is, as the cold SST biases appear in the TNA, the warm SST biases also occur in the SEP. This indicates that if climate models cannot succeed in simulating the TNA variability, they will also fail at least partially in the SEP. Our coupled model experiments show that the cold SST bias in the TNA results in a weakening of the Hadley-type circulation from the TNA to the SEP. This meridional circulation reduces the South Pacific subtropical anticyclone and the associated subsidence, which in turn leads to a reduction of low clouds, a weakening of the easterly trade wind, and thus an increase of the warm SST bias in the SEP.

1. Introduction

In observations, the large asymmetry of SST about the equator is one of the most striking climate features in the eastern tropical Pacific. In this region, SST is higher to the north and lower to the south throughout the seasonal cycle. In association with the cool SST, the SEP is characterized by large-scale subsidence, extensive and persistent stratocumulus clouds. Under the subsidence, surface winds evaporate water vapor from the ocean, but the atmospheric inversion prevents the moist air from rising to significant elevations. A thin layer of stratus or stratocumulus clouds form at the base of the inversion and shield the ocean surface from solar radiation. Light precipitation (drizzle) under the stratus cloud deck is also a prominent regional feature. The subsidence over the SEP during the austral summer (boreal winter) is suggested to be related to the monsoonal heating over South America. *Rodwell and Hoskins* [2001] demonstrate by using an atmospheric model that Rossby wave response to heating associated with the South American monsoon system interacting with the midlatitude westerlies produces descending motion to the west of the South American heating (i.e., over the SEP). *Richter and Mechoso* [2008] demonstrate that the westerly wind impinging on the Andes Mountains contributes to sinking along the equatorward-sloping isentropes thus promoting subsidence over the SEP. This process must be at work in all seasons, but the effects would be primarily confined near the coastal region.

Most climate models fail to reproduce the observed seasonal cycle in the eastern tropical Pacific [*Szoeke and Xie*., 2008; *Mechoso et al*., 1995]. One of the most common errors in climate models is a warm SST bias in the SEP, with the warm bias extending thousands of kilometers off the coast of Peru. The warm SST bias in the SEP may have multiple sources. One is the shortage of model low-level stratus clouds in the region, so that an excessive amount of solar radiation reaches the sea surface [*Ma et al*., 1996; *Meehl et al*., 2005]. Near the South American coast, warm SSTs could be associated with weak coastal upwelling due to the underestimation of alongshore surface winds [*Huang and Schneider*, 1995; *Schneider et al*., 1997]. Furthermore, Current Ocean GCMs do not have high enough resolution to resolve vigorous mesoscale eddies which spread the cold signals from the coastal upwelling zone into the open ocean [*Colbo and Weller*, 2007]. Overall, these studies primarily focus on the local influence on the SST bias in the SEP.

Wang et al. [2010] suggested that there is an interhemispheric influence of the Atlantic Warm Pool (AWP) on the SEP. The AWP is a large body of warm water comprising the Gulf of Mexico, Caribbean Sea, and

This is an open access article under the terms of the Creative Commons Attribution-NonCommercial-NoDerivs License, which permits use and distribution in any medium, provided the original work is properly cited, the use is non-commercial and no modifications or adaptations are made.

© 2014. The Authors.

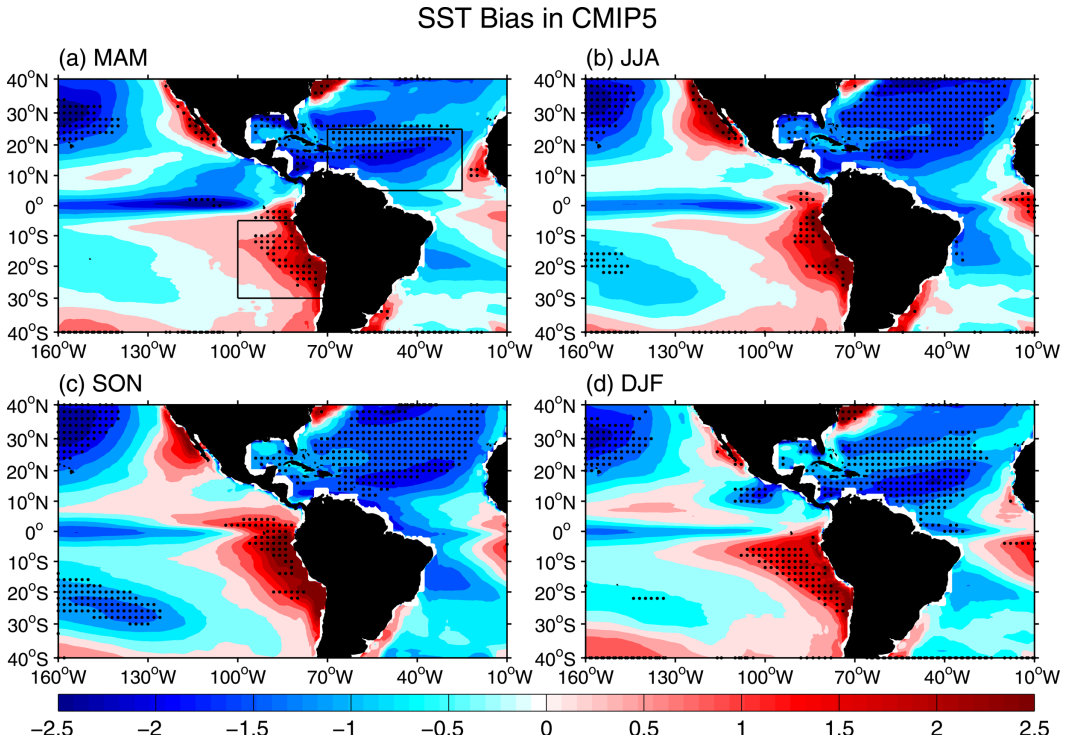

Figure 1. (a) Spring (MAM), (b) summer (JJA), (c) autumn (SON), and (d) winter (DJF) mean SST bias averaged over 18 CMIP5 models. Unit is °C. The SST bias is calculated by subtracting the ERSST from the long-term mean-coupled model SST. The black boxes in (a) denote the regions for the scatterplot in Figure 2. The dotted region denotes that all 18 models have the detectable biases. The detectable bias in each model means that the SST bias is significant at 95% confidence level based on the t-test.

western tropical North Atlantic. In extent, the AWP varies on seasonal, interannual, and multidecadal time scales with maximum size that is almost 3 times the smallest one when it is as its annual low in the boreal summer/fall [*Wang et al.*, 2008]. During the season of maximum extent, a strong Hadley-type circulation is established with ascending branch near the AWP and subsidence over the SEP. On longer time scale, they pointed out that an anomalously large (small) AWP during the boreal summer results in a strengthening (weakening) of the Hadley-type circulation with enhanced descent (ascent) over the SEP. Climate models in CMIP5 further show that virtually all of coupled models have significant, but synchronous biases in the SEP and TNA Oceans (Figure 1). The bias here is defined as the SST difference between the CMIP5 model and observation (ERSST, see section 2). These biases manifest themselves as the SST in the SEP Ocean being too warm and SST in the TNA being too cold. The magnitude of these biases can be as large as 3°C or more, resulting in a significant distortion of the coupled annual cycle of the tropical eastern Pacific and Atlantic in these models. Given the magnitude of these biases and the interhemispheric influence of the AWP on the SEP, an interesting question arises: Is it possible that the warm bias in the SEP may be attributed, at least partially, to the cold biases in the TNA?

By focusing on the SST biases in CMIP5 climate models [*Wang et al.*, 2014], we find that there is a link between the cold bias in the TNA and the warm bias in the SEP. The purpose of the present paper is to demonstrate that the cold bias in the TNA does contribute to the warm bias in the SEP by performing sensitivity model experiments. In section 2, we describe the models and data sets used in this paper. The relationship between the TNA cold bias and the SEP warm bias in CMIP5 models is briefly reviewed and described in section 3. In section 4, we present the coupled ocean and atmosphere model response to the TNA cold SST bias. A short discussion and summary are given in section 5.

2. Coupled Models and Methods

This study is based on output from 18 Coupled Model Intercomparison Project Phase 5 (CMIP5) GCM runs corresponding to the "historical" collection of simulations [*Taylor et al.*, 2012]. The historical run is forced by observed atmospheric composition changes which reflect both anthropogenic (green house gases) and

© 2014. The Authors.

Table 1. The 18 Models Involved in This Study and Their Sponsor, Country, and Names

Sponsor, Country	Model Name
Commonwealth Scientific and Industrial Research Organization (CSIRO), Australia	ACCESS1.0
Canadian Center for Climate Modeling and Analysis, Canada	CanESM2
National Center for Atmospheric Research (NCAR), USA	CCSM4
Météo-France/Centre National de Recherches Météorologiques, France	CNRM-CM5
European Earth System Model, EU	EC-EARTH
U.S. Department of Commerce/National Oceanic and Atmospheric Administration (NOAA)/Geophysical Fluid Dynamics Laboratory (GFDL),USA	GFDL-CM3
	GFDL-ESM2G
	GFDL-ESM2M
Met office Hadley Centre, UK	HadCM3
	HadGEM2-CC
	HadGEM2-ES
Institute Pierre Simon Laplace, France	IPSL-CM5A-MR
	IPSL-CM5B-LR
Center for Climate System Research (University of Tokyo), National Institute for Environmental Studies, and Frontier Research Center for Global Change (JAMSTEC), Japan	MIROC5
Max Planck Institute for Meteorology, Germany	MPI-ESM-LR
	MPI-ESM-P
Meteorological Research Institute, Japan	MRI-CGCM3
Norwegian Climate Centre, Norway	NorESM1-M

natural sources (volcanic influences, solar forcing, aerosols and emissions of short-lived species, and their precursors) and, for the first time, including time-evolving land cover. These historical runs cover much of the industrial period from the mid-19th century to the near present. Variables SST, zonal wind, and meridional wind at 850 hPa spanning from 1900 to 2005 are used in this study. The modeling center, country, and name are listed in Table 1.

Observational SST data from the NOAA Extended Reconstruction Sea Surface Temperature version 3 (ERSST v3) [*Smith and Reynolds,* 2004] was used to validate the variability of the coupled GCM simulations. The temporal coverage is from January 1854 to the present and it has a spatial resolution on a $2^\circ \times 2^\circ$ grid. Because we are interested only in large-scale features, unless otherwise specified, all model outputs and ERSST data are interpolated to a $1^\circ \times 1^\circ$ grid. The SST bias here is defined as the climatological SST difference between the CMIP5 model and ERSST. The averaged time period chosen here is from 1900 to 2005.

To investigate the physical mechanism connecting the TNA and SEP SST biases, we conduct two sensitivity experiments by using the fully coupled NCAR Community Earth System Model (CESM1.0.4) [*Meehl et al*., 2012]. The atmospheric component in this version of CESM is the Community Atmospheric Model version 4 (CAM4) having horizontal resolution of $2.5^\circ \times 1.875^\circ$ on a finite volume grid and 26 hybrid levels in the vertical. The ocean model is a version of the Parallel Ocean Program (POP) developed at Los Alamos National Laboratory with 1° horizontal resolution and enhanced meridional resolution ($1/3^\circ$) in the equatorial tropics and the North Atlantic and with 60 vertical levels. The fully coupled control simulation has been integrated for 1500 years without apparent climate shifts. The first experiment is the control restoring run and named as RES_CTR. The ocean and atmosphere are fully coupled except in the TNA region (0°N-30°N and from the east to west coast) where we restore the model-produced SST to the climatological SST of CESM1.0.4 at every integration step. Here the CESM1.0.4 climatological SST is obtained by averaging the last 100 years of 1500 years long-term fully coupled CESM1.0.4 simulation. Therefore, the atmosphere model can only see the prescribed climatological SST over the TNA region instead of the ocean model output. The second experiment is configured the same as the first experiment but with the SST in the TNA region restoring to the CESM1.0.4 climatological SST added with the monthly SST cooling bias in the region of 0°N-30°N and from the east to west coast. The monthly SST cooling bias over the TNA Ocean is obtained by subtracting the climatological ERSST from the CMIP5 ensemble mean SST, as shown in Figure 1. This experiment is named as RES_TNAbias. Both the RES_CTR and RES_TNAbias experiments are integrated for 100 years. The difference averaged in the last 30 years between the RES_TNAbias and RES_CTR runs is taken as the response to the cold bias in the TNA.

3. Relationship Between the TNA Cold Bias and SEP Warm Bias in CMIP5 Models

The model simulations in CMIP5 show a large cold SST bias in the TNA, with ensemble mean amplitude up to 2.5°C (Figures 1a–1d). This cold bias persists throughout the whole year without a significant seasonal

© 2014. The Authors.

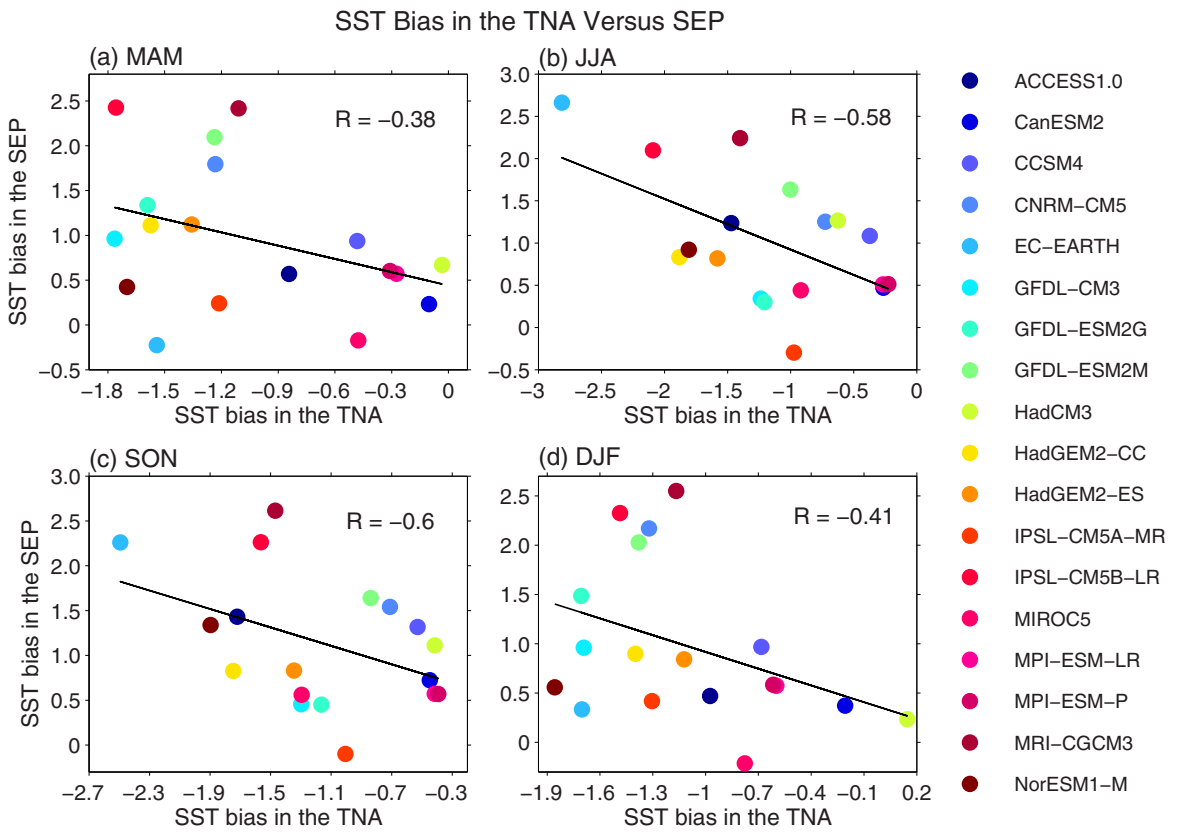

Figure 2. Scatterplot of the spring (a), summer (b), autumn (c), and winter (d) mean tropical North Atlantic SST bias (5°N–25°N, 70°W–25°W) versus southeastern Pacific SST bias (30°S–5°S, 100°W-coast). Unit is °C. The intermodel correlations in different seasons are shown in the upper right corner of each plot. The intermodel correlations are significant at 80% confidence level for (a) MAM and (d) DJF, and are significant at 90% confidence level for (b) JJA and (c) SON based on the t-test.

variability. Here, the SST bias is calculated by subtracting the climatological ERSST from the ensemble mean CMIP5 models. For the spatial structure, the TNA cold bias tilts northeastward to the eastern subtropics, which coincides with the trade wind location and the subduction path. This implies that the cold bias may be related to the latent heat bias as a result of the overestimated trade wind strength [*Liu et al.* 2012] or associated with the bias in the subtropics which propagates southward due to the subduction or advection process of subtropical gyre. These possible mechanisms causing the SST bias in the TNA region will be the subject of future work. Then we turn attention to the SEP where a large warm SST bias exists in excess of 2.5°C off the coast of Peru (Figures 1a–1d). This warm bias extends northward to the south of the equator in the eastern tropical Pacific and northwestward to the equator around 100°W. Similar to the cold bias in the TNA, the SEP warm SST bias is significant in all models and occurs in all seasons.

To further examine the linkages of SST bias between the TNA and SEP, we plot these biases in a scatterplot format using 18 CMIP5 models. As shown in Figures 2a–2d, the TNA cold bias is negatively correlated with the SEP warm bias in all seasons. It means that as a cold SST bias appears in the TNA, a warm SST bias occurs in the SEP. This intermodel negative correlation between the TNA and SEP SST biases has higher values in summer and autumn (Figures 2b and 2c), with a correlation up to −0.58 and −0.60, respectively. In contrast, the correlations are −0.41 in winter (Figure 2d) and −0.38 in spring (Figure 2a). This interhemispheric SST bias relation shows a remarkable resemblance to the AWP-SEP teleconnection proposed by *Wang et al.* [2010], supporting the possibility that the SST bias in the SEP may be partially attributed to the remote effect of the large SST biases in the TNA.

In order to investigate the physical linkages between TNA bias and SEP bias further, we select the three models with the largest (EC-EARTH, IPSL-CM5B-LR, and MRI-CGCM3) and the three models with the smallest (CanESM2, MPI-ESM-LR, and MPI-ESM-P) TNA-SEP bias dipole. The SST and 850 mb wind differences between the large and small TNA-SEP dipole bias models are exhibited in Figure 3a. As expected, there is a

© 2014. The Authors.

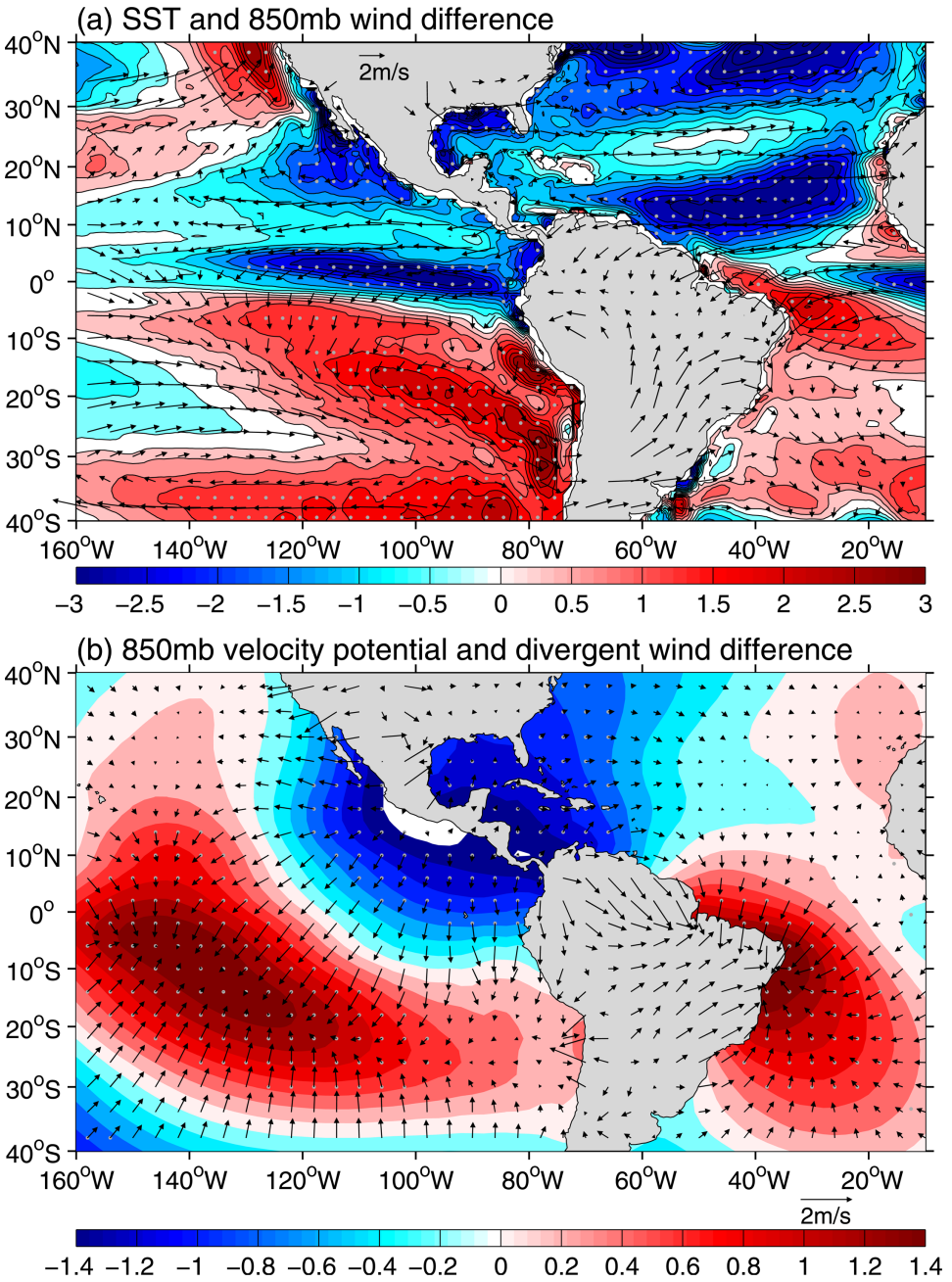

Figure 3. (a) SST (°C) and 850 mb wind (m/s) differences between the large TNA-SEP dipole bias models (EC-EARTH, IPSL-CM5B-LR, and MRI-CGCM3) and the small TNA-SEP dipole bias models (CanESM2, MPI-ESM-LR, and MPI-ESM-P). (b) Same as (a) but for the 850 mb velocity potential (10^6 m^2s^{-1}) and divergent wind (m/s) differences. The dotted region denotes that the difference is significant at 90% confidence level based on the t-test.

cold SST anomaly in excess of 3°C over the TNA and a warm SST anomaly on the order of 2.5°C off the coast of Peru. The wind difference is characterized by an anticyclonic wind over the TNA in response to the cold SST, which is consistent with previous studies [*Wang and Enfield*, 2001; *Zhang and Wang*, 2012]. Note that the northeast wind branch is extremely strong, which extends to the eastern tropical Pacific, and induces northeasterly wind anomalies north of the equator, northerly cross-equatorial winds, and northwesterly winds (due to Coriolis force) south of the equator. This C-shaped wind anomaly coincides well with the eastern Pacific north-south dipole SST pattern, suggesting an important role of the wind-evaporation-SST (WES) feedback. It is also confirmed by the surface latent heat flux difference which favors the SEP warm anomaly

© 2014. The Authors.

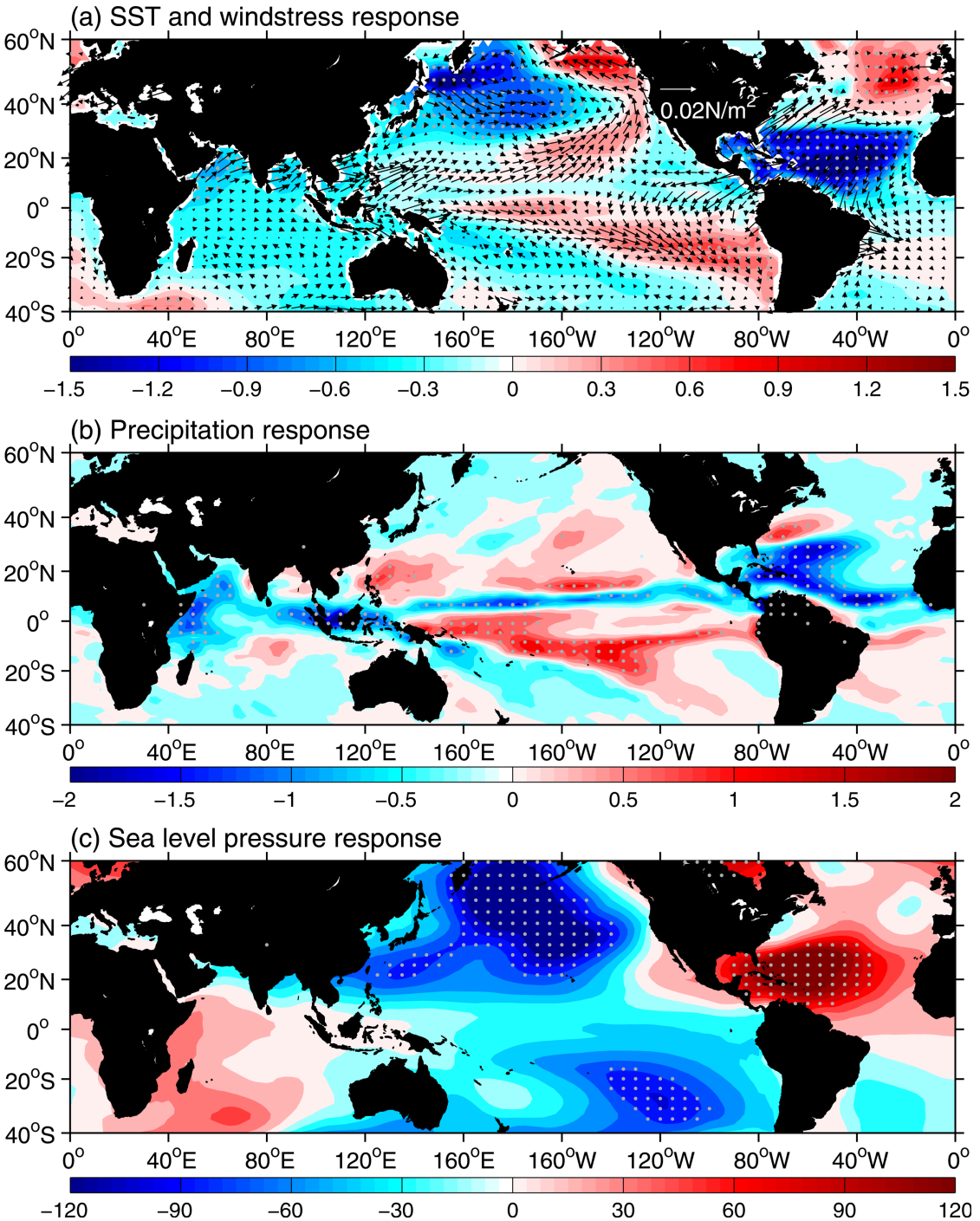

Figure 4. (a) SST (°C) and wind stress (N/m^2), (b) precipitation (mm/day) and (c) sea level pressure (Pa) differences between the RES_TNAbias and RES_CTRL runs. The dotted region denotes that the difference is significant at 90% confidence level based on the t-test.

(not shown). The impact of the anomalous TNA cooling on the SEP can be further examined by inspecting the difference between the velocity potential and divergent wind at 850 mb, as displayed in Figure 3b. It is clearly seen that the cold TNA is associated with divergent flow of the lower troposphere that crosses the equator into the SEP. That is, the anomalous Hadley-type circulation shows descent in the western TNA and ascent over the SEP. In view of the mean atmospheric circulation, the effect of the anomalous SST cooling in the TNA is to weaken the regional Hadley-type circulation from the TNA region to the SEP. This

© 2014. The Authors.

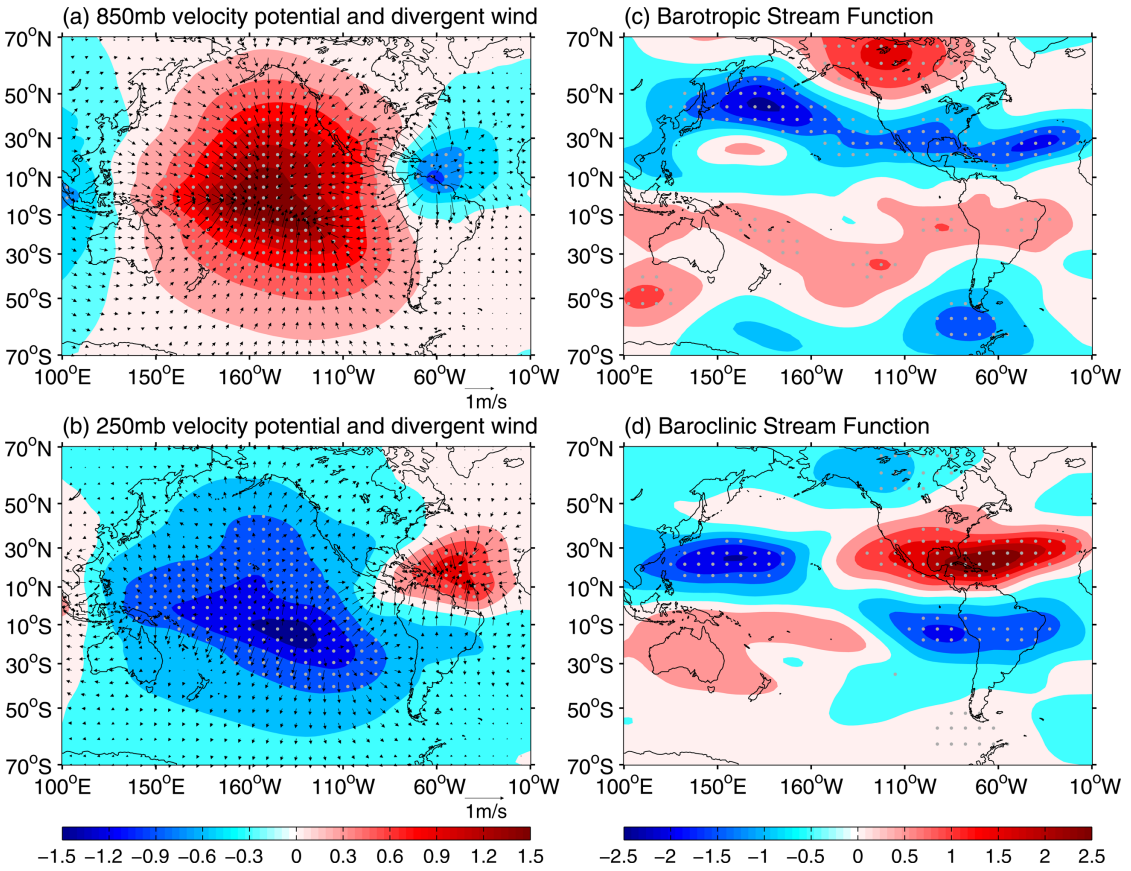

Figure 5. (a) 850 mb velocity potential (10^6 m^2s^{-1}) and divergent wind (m/s), (b) 250 mb velocity potential (10^6 m^2s^{-1}) and divergent wind (m/s), (c) barotropic stream function (10^6 m^2s^{-1}) and (d) baroclinic stream function (10^6 m^2s^{-1}) differences between the RES_TNAbias and RES_CTRL runs. The dotted region denotes that the difference is significant at 90% confidence level based on the t-test.

meridional circulation weakens the South Pacific subtropical anticyclone and the easterly trade winds near the equatorial eastern/central Pacific. The weakened easterly trade winds and subsidence eventually affect the SEP SST.

Note that the SST and wind differences are calculated between the large and small TNA-SEP dipole SST bias models, which may also include the effects of other variability in regions such as the tropical eastern south Pacific and Africa. Therefore, next we use the fully coupled CESM1.0.4 model experiments to demonstrate the influences associated with variability in the circulation due to the TNA cold bias.

4. Coupled Model Response to the TNA Cold SST Bias

The annual mean SST response in the eastern tropical Pacific is characterized by a north-south dipole, with the cold and warm anomaly north and south of the equator, respectively (Figure 4a). The magnitude of the SEP SST warm response is as high as 0.6°C, which accounts for 25%–30% of the SEP warming bias presented in Figure 1. This suggests that the SST bias in the SEP is partially attributed to the remote effect of the cold SST biases in the TNA. In contrast to the SEP warm bias in CMIP5 models which is mainly confined east of 110°W, the modeling warm response in the SEP Ocean occupies a broad region, which extends northwestward from the coastal region into the central and western equator. This may be due to the positive effect of Bjerknes and WES feedbacks. The former tends to propagate the warm anomaly from the eastern Pacific to the western Pacific and the latter plays an important role for the warm SSTs propagating from the extratropics to the tropics. Our model results here suggest that the cold TNA SST can induce a warm-pool El Niño events, with a center of action located in the central Pacific. This is consistent with *Ham et al.* [2013] who argued that the identification of temperature anomalies in the TNA could help to forecast the development of different types of El Niño events.

© 2014. The Authors.

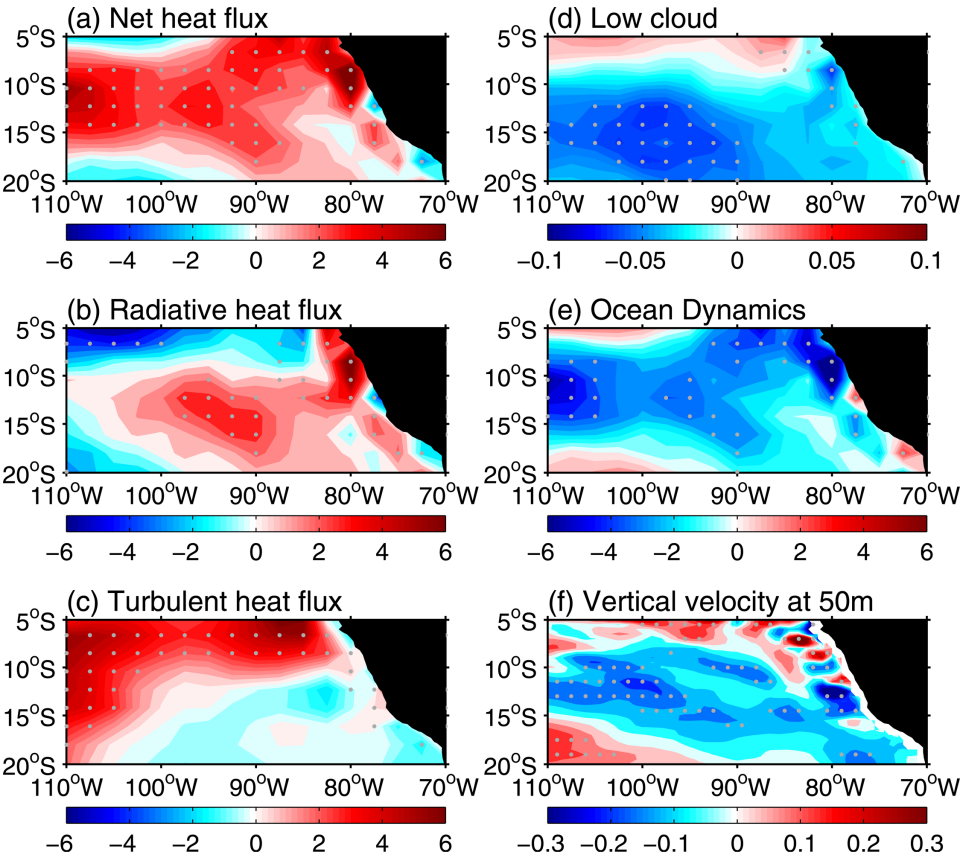

Figure 6. Heat budget analysis over the SEP region. (a) Net heat flux (W/m^2), (b) radiative heat flux (W/m^2), (c) turbulent heat flux (W/m^2), (d) low clouds (%), (e) ocean dynamics (W/m^2), and (f) vertical velocity at 50m (10^{-3} m/s) differences between the RES_TNAbias and RES_CTRL runs. The dotted region denotes that the difference is significant at 90% confidence level based on the t-test.

The SEP warm SST anomaly can be generated as follows: the TNA cold bias suppresses convection and rainfall near the AWP region (Figure 4b), producing a surface high extending to the eastern tropical North Pacific, a Rossby wave response (Figure 4c). Over the eastern tropical Pacific, this anomalous high induces northeasterly wind anomalies north, northerly cross-equatorial winds, and northwesterly winds south of the equator (Figure 4a). This C-shaped wind anomaly generates a dipole SST anomaly (warm and cold south and north of the equator, respectively) through changes in evaporation. It appears that this coupled WES feedback, which has been extensively studied in relation to tropical Atlantic variability [*Xie and Carton*, 2004], acts to amplify the SST dipole. The northwesterly wind south of the equator also reduces the coastal upwelling, which also partly contributes to the SEP warm anomaly. The formation of cross-basin nondivergent wind is primarily due to the weakening of the Hadley-type circulation from the AWP region to the SEP as a result of the cold SST bias imposed in the TNA region. As exhibited in Figures 5a and 5b, the TNA cooling is associated with a divergent circulation in the low troposphere that crosses the equator into the South Pacific and vice versa for the upper troposphere. This meridional circulation reduces the South Pacific subtropical anticyclone (Figure 4c) and the associated subsidence, which in turn leads to a reduction of low clouds, a weakening of the easterly trade wind and thus an increase of the SST.

A heat budget analysis in the SEP region further confirms the physical mechanisms discussed above. It can be seen that the SEP warming is mainly associated with the surface heat flux heating (Figure 6a), whereas the ocean dynamics which is mainly contributed from the temperature advection by the anomalous vertical current (Figure 6f) play a damping role except in the southwestern coastal region (Figure 6e). The positive contribution of heat flux arises from both the surface radiative and turbulent heat fluxes (Figures 6b and 6c). The warm effect of radiative heat flux is dominant by the short wave radiation as a result of a reduction of low clouds (Figure 6d). As discussed above, the regional Hadley-type circulation from the AWP region to the SEP is significantly weakened, leading to a reduction of the SEP subsidence, a decrease of the

© 2014. The Authors.

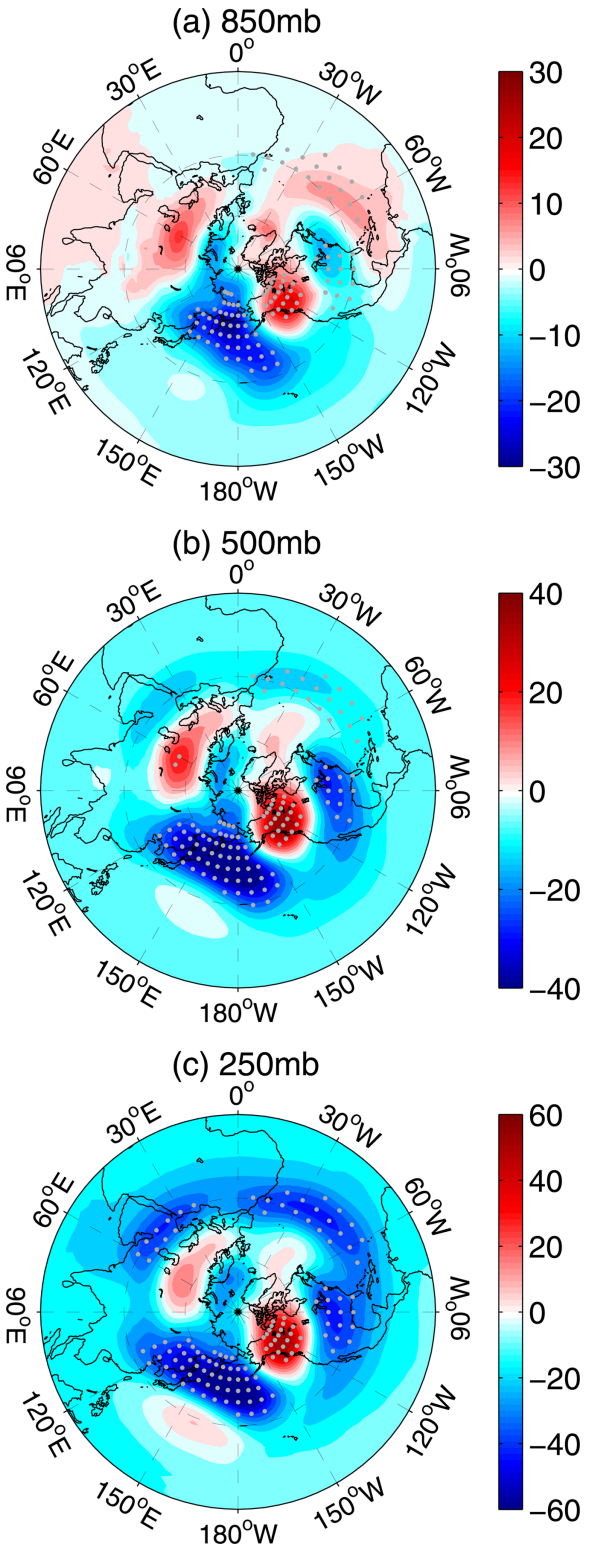

Figure 7. Geopotential height difference between the RES_TNAbias and RES_CTRL runs at (a) 850 mb, (b) 500 mb, and (c) 250 mb. Unit is m. The dotted region denotes that the difference is significant at 90% confidence level based on the t-test.

stratocumulus, and thus an increase of the downward shortwave radiation. The turbulent heat flux is primarily attributed to the latent heat flux due to the weakening of the trade wind (Figure 4a), while the sensible heat flux is of secondary importance (not shown).

There are both local and remote atmospheric responses to the TNA cold bias. Here the baroclinic and barotropic stream functions are calculated as $\psi_c=(\psi_{850mb}-\psi_{250mb})/2$ and $\psi_t=(\psi_{850mb}+\psi_{250mb})/2$, respectively. As shown in Figure 5d, the baroclinic stream function response shows a pair of anticyclones: one in the TNA and northeastern Pacific and the other in the SEP and South America. This model response is largely consistent with *Gill*'s [1980] solution to a cooling anomaly slightly north of the equator [*Heckley and Gill*, 1984]. Different from the atmosphere model response in *Wang et al.* [2010], there is also a strong pair of cyclones in the western Pacific. This can be interpreted as follows: the SEP warm anomaly gradually propagates to the western and central Pacific due to the positive Bjerknes and WES feedbacks, which induces a large amount of precipitation there (Figures 4a and 4b). The heating anomaly over the western tropical Pacific eventually induces a baroclinic response represented by a pair of cyclones. In addition to the baroclinic response, the tropical Pacific warming also triggers the classical Pacific North America (PNA) pattern, which is largely barotropic [e.g., *Horel and Wallace*, 1981]. The PNA teleconnection is clearly seen from the barotropic stream function (Figure 5c) and the geopotential height responses (Figures 7a–7c). As shown in Figure 7, the structure of the middle latitude geopotential response shares great similarities in the upper (Figure 7c), middle (Figure 7b), and low (Figure 7a) layers, with a low pressure in the North Pacific Ocean, a high pressure in the North America land, and a low pressure in the south United States, representing a positive phase of the PNA response which is largely barotropic.

Consistent with the atmosphere model responses in an AGCM [*Wang et al.*, 2010] and in a simple atmospheric model [*Lee et al.*, 2009], the barotropic component also shows a pattern of alternating

© 2014. The Authors.

high and low centers from the TNA to high latitudes (Figure 5c). In response to the PNA teleconnection, the surface wind in the North Pacific Ocean is characterized by a cyclone, which generates a horseshoe-like SST pattern, with a cooling in the northwestern and central Pacific and a warming in the east extending northwest into the subpolar ocean and southwest into the subtropics (Figure 4a). This SST response is mainly due to the surface heat flux and temperature advection by the anomalous meridional current (not shown). The eastern warming is also propagated to the western tropics by the positive WES feedback as seen in other models [*Zhang et al*., 2011a, 2011b], which in turn reinforces the tropical Pacific warming, the western Pacific baroclinic cyclones, and the subsequent PNA teleconnection. Therefore, the TNA cold bias not only induces SST response in the SEP, but also induces significant SST responses in the North Pacific. We also find that there is a close relationship between the TNA cold bias and the North Pacific cold bias in CMIP5 models. However, that is beyond the scope of this study, but subject to future work.

5. Discussions and Summary

The results presented here suggest that the SEP warm bias in coupled ocean-atmosphere models may come from remote processes, in addition to the local sources. The leading candidates for the local influence are regional feedbacks between stratocumulus clouds, surface winds, upwelling, coastal currents, and SST in the SEP region, which are poorly represented in many climate models. On the other hand, the SEP warm bias may contain a significant component that comes from the large biases in the TNA via remote processes. This remote effect can be seen in CMIP5 models: those models with colder TNA bias have warmer SEP bias, and vice versa. We use the numerical experiments of CESM1.0.4 to show that as much as 30% of the warm SST bias in the SEP can be attributed to the cold SST biases in the TNA. If this assessment is accurate, then the remote impact of the TNA biases is too significant to be ignored. This means that effort of reducing coupled model biases in the SEP should take into consideration not only the local processes, but also the remote influence, especially in the TNA.

The detailed mechanism through which the TNA biases affect the SEP is briefly explored in this study. The cold bias in the TNA region weakens the Hadley-type circulation from the AWP region to the SEP. The TNA cooling is associated with a divergent (convergent) circulation in the low (upper) troposphere that crosses the equator into the South Pacific. This meridional circulation and the associated subsidence reduce the South Pacific subtropical anticyclone, and in turn lead to a reduction of low clouds, a weakening of the easterly trade wind and thus an increase of the SST. This indicates that if models cannot succeed in simulating the TNA variability, they will also fail at least partially over the SEP.

Acknowledgments

The CMIP5 data for this paper are available through the Earth System Grid-Center for Enabling Technologies (ESG-CET), on the page http://pcmdi9.llnl.gov/. The ERSST data are available at NOAA's Earth System Research Laboratory, on the page http://www.esrl.noaa.gov/psd/data/gridded/. Data set: NOAA Extended Reconstructed SST. Data set name: sea surface temperature. The model output used in this paper is available upon request. This work was supported by grants from National Oceanic and Atmospheric Administration (NOAA) Climate Program Office, the base funding of NOAA Atlantic Oceanographic and Meteorological Laboratory (AOML), National Science Foundation, and National Basic Research Program of China (2010CB950500 and 2013CB430301). The findings and conclusions in this report are those of the author(s) and do not necessarily represent the views of the funding agency.

References

Colbo, K., and R. A. Weller (2007), The variability and heat budget of the upper ocean under the Chile-Peru stratus, *J. Mar. Res.*, *65*, 607–637.

De Szoeke, P. S., and S.-P. Xie (2008), The tropical eastern Pacific seasonal cycle: Assessment of errors and mechanisms in IPCC AR4 coupled ocean–atmosphere general circulation models, *J. Clim.*, *21*, 2573–2590.

Gill, A. E. (1980), Some simple solutions for heat-induced tropical circulation. *Q. J. R. Meteorol. Soc.*, *106*, 447–462.

Ham, Y.-G., J.-S. Kug, J.-Y. Park, and F.-F. Jin (2013), Sea surface temperature in the north tropical Atlantic as a trigger for El Niño/Southern Oscillation events. *Nat. Geosci.*, *6*, 112–116.

Heckley, W. A., and A. E. Gill (1984), Some simple analytic solutions to the problems of forced equatorial long waves. *Q. J. R. Meteorol. Soc.*, *110*, 203–217.

Horel, J. D., and J. M. Wallace (1981), Planetary-Scale atmospheric phenomena associated with the southern oscillation. *Mon. Weather Rev.*, *109*, 813–829.

Huang, B., and E. K. Schneider (1995), The response of an ocean general circulation model to surface wind stress produced by an atmospheric general circulation model. *Mon. Weather Rev.*, *123*, 3059–3085.

Lee, S.-K., C. Wang, and B. E. Mapes (2009), A simple atmospheric model of the local and teleconnection responses to tropical heating anomalies. *J. Clim.*, *22*, 272–284.

Liu, H., C. Wang, S.-K. Lee, and D. B. Enfield (2012), Atlantic warm pool variability in the IPCC-AR4 CGCM simulations. *J. Clim.*, *25*, 5612–5628.

Ma, C.-C., C. R. Mechoso, A. W. Robertson, and A. Arakawa (1996), Peruvian stratus clouds and tropical Pacific circulation: A coupled ocean–atmosphere GCM study. *J. Clim.*, *9*, 1635–1645.

Mechoso, C. R. et al. (1995), The seasonal cycle over the tropical Pacific in coupled ocean-atmosphere general circulation models, *Mon. Weather Rev.*, *123*, 2825–2838.

Meehl, G. A., C. Covey, B. McAvaney, M. Latif, and R. J. Souffer (2005), Overview of the coupled model intercomparison project. *Bull. Am. Meteorol. Soc.*, *86*, 89–93.

Meehl, G. A., W. M. Washington, J. M. Arblaster, A. Hu, H. Teng, C. Tebaldi, W. G. Strand, and J. B. White (2012), Climate system response to external forcings and climate change projections in CCSM4. *J. Clim.*, *25*, 3661–3683.

Richter, I., and C. R. Mechoso (2008), What determines the position and intensity of the South Atlantic anticyclone in austral winter?: An AGCM study, *J. Clim.*, *21*, 214–229.

Rodwell, M. J., and B. J. Hoskins (2001), Subtropical anticyclones and summer monsoons, *J. Clim.*, *14*, 3192–3211.

Schneider, E. K., Z. Zhu, B. S. Giese, B. Huang, B. P. Kirtman, J. Shukla, and J. A. Carton (1997), Annual cycle and ENSO in a coupled ocean–atmosphere model. *Mon. Weather Rev.*, *125*, 680–702.

© 2014. The Authors.

Smith, T. M., and R. W. Reynolds (2004), Improved extended reconstruction of SST (1854–1997), *J. Clim.*, *17*, 2466–2477.
Taylor, K. E., R. J. Stouffer, and G. A. Meehl (2012), An overview of CMIP5 and the experiment design. *Bull. Am. Meteorol. Soc.*, *93*, 485–498.
Wang, C., and D. B. Enfield (2001), The tropical western hemisphere warm pool, *Geophys. Res. Lett.*, *28*, 1635–1638.
Wang, C., S.-K. Lee, and D. B. Enfield (2008), Atlantic warm pool acting as a link between Atlantic multidecadal oscillation and Atlantic tropical cyclone activity, *Geochem. Geophys. Geosyst.*, *9*, Q05V03, doi:10.1029/2007GC001809.
Wang, C., S.-K. Lee, and C. R. Mechoso (2010), Interhemispheric influence of the Atlantic warm pool on the Southeastern Pacific. *J. Clim.*, *23*, 404–418.
Wang, C., L. Zhang, S.-K. Lee, L. Wu, and C. R. Mechoso (2014), A global perspective on CMIP5 climate model biases. *Nat. Clim. Change*, *4*, 201–205.
Xie, S.-P., and J. A. Carton (2004), Tropical Atlantic variability: Patterns, mechanism, and impacts. Earth climate: The ocean–atmosphere interaction. *Geophys. Monogr.*, *147*, 121–142.
Zhang, L., and C. Wang (2012), Remote influences on freshwater flux variability in the Atlantic warm pool region. *Geophys. Res. Lett.*, *39*, L19714, doi:10.1029/2012GL053530.
Zhang, L., L. Wu, and J. Zhang (2011a), Coupled ocean-atmosphere responses to recent freshwater flux changes over the Kuroshio-Oyashio extension region, *J. Clim.*, *24*, 1507–1524.
Zhang, L., L. Wu, and J. Zhang (2011b), Simulated response to recent freshwater flux change over the gulf stream and its extension: Coupled ocean–atmosphere adjustment and Atlantic–Pacific teleconnection, *J. Clim.*, *24*, 3971–3988.

© 2014. The Authors.